Forestry: An International Journal of Forest Research, 2026, 99(3), cpag041
https://doi.org/10.1093/forestry/cpag041
Published: 24 May 2026
Review

Institute of Chartered Foresters
OXFORD

Contrasting Sentinel-2 based biophysical constraints of growth, productivity, and stem water dynamics in thinning trials of two mediterranean pines

Antonio M. Cachinero-Vivar[1,2,*], Enrique P. Sánchez-Cañete[2,3], Andrew S. Kowalski[2,3], Óscar Pérez-Priego[1,2,*]

[1]Department of Forest Engineering, School of Agriculture and Forestry, University of Córdoba, Laboratory of Dasometry and Forest Management, Edif. Leonardo da Vinci, Campus de Rabanales s/n, Córdoba 14071, Spain
[2]Andalusian Institute Earth System Research IISTA-CEAMA, Granada 18006, Spain
[3]Applied Physics Department, Faculty of Science, University of Granada, Granada 18071, Spain

*Corresponding authors: Antonio M. Cachinero-Vivar, Department of Forest Engineering, School of Agriculture and Forestry, University of Córdoba, Laboratory of Dasometry and Forest Management, Edif. Leonardo da Vinci, Campus de Rabanales s/n, 14071 Córdoba, Spain. E-mail: o02cavia@uco.es; Óscar Pérez-Priego, Department of Forest Engineering, School of Agriculture and Forestry, University of Córdoba, Laboratory of Dasometry and Forest Management, Edif. Leonardo da Vinci, Campus de Rabanales s/n, Córdoba 14071, Spain. E-mail: g72pepro@uco.es

Abstract

Thinning alters forest structure and functioning, yet its effects on canopy biochemistry, growth, carbon uptake and hydraulic dynamics remain poorly quantified across spatial and temporal scales. We combined Sentinel-2 PROSAIL inversion with explicit uncertainty propagation to derive monthly canopy traits in paired thinned and control stands of *Pinus sylvestris* and *P. nigra*, integrating these with high-frequency eddy-covariance GPP, maximum daily stem-shrinkage (MDS), and decadal basal area increment (BAI) from tree-ring records. Thinning reduced canopy density, pigment content, and albedo, indicating a shift in stand optical properties toward a more open but less reflective canopy structure. Functionally, thinning increased long-term basal-area increment by ∼90% in *P. sylvestris* and ∼35% in *P. nigra*, but reduced spring GPP by up to ∼9 μmol CO_2 m^{-2} s^{-1} and intensified summer hydraulic drawdown (ΔMDS ≈ -60 μm). Trait–function models explained 61% of BAI, 85% of GPP, and 30% of MDS variance, indicating distinct biophysical controls across response variables: leaf structural traits (especially LMA) was the strongest predictor of long-term growth, canopy architecture primarily explained seasonal productivity, and pigment–structure interactions contributed most to stem-water dynamics. This multi-scale, uncertainty-aware framework shows how integrated satellite, flux-tower and dendrochronological measurements can robustly detect and interpret thinning impacts in Mediterranean pine forests.

[†]Handling editor: Dr. Fabian Fassnacht
Received: 28 July 2025. **Revised:** 10 April 2026. **Accepted:** 24 April 2026

Graphical abstract

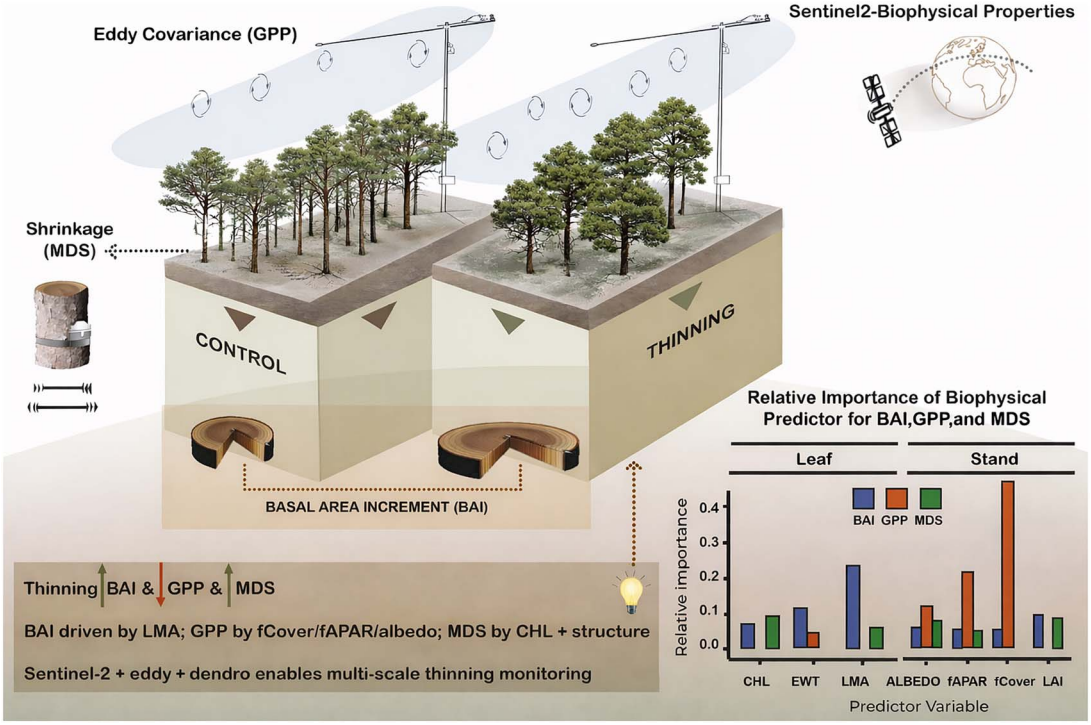

Keywords radiative transfer modelling (PROSAIL), Sentinel-2 hybrid retrievals, thinning trials, gross primary production (GPP), Eddy-covariance flux measurements, maximum daily stem shrinkage (MDS), high-resolution dendrometry

Introduction

The Mediterranean Basin is recognized as a climate-change hotspot where rising temperatures and declining precipitation converge to generate more severe droughts and wildfires, and increase tree mortality (Cramer *et al.* 2001, Rustad 2008, Manning *et al.* 2018, Silva and Lambers 2021). Plantation forests dominated by *Pinus* species cover ∼9 million hectares across southern Europe and constitute a cornerstone of regional carbon budgets and rural economies (Vadell *et al.* 2016). Maintaining their productivity and ecosystem services is therefore an urgent priority for both forest managers and policymakers (Manning *et al.* 2018).

Because of climate change, silvicultural thinning—the selective removal of competing stems—has widely been employed to redistribute resources, improve stand stability, and reduce fuel loads. Meta-analyses show that thinning can mitigate drought stress by lowering stand-level transpiration and increasing soil moisture (Sohn *et al.* 2016). However, heavy thinning also removes photosynthetically active foliage and can alter microclimate, potentially constraining canopy-scale carbon uptake (Davi *et al.* 2008). Striking the right balance between growth release and ecosystem functionality remains a practical challenge, particularly under intensifying drought.

Recent trait-based research has revealed coordinated shifts along the acquisitive–conservative spectrum when stands are thinned. In Mediterranean pine plantations, thinning lowered leaf mass per area while increasing hydraulic conductivity and sap-flow rates, thereby enhancing short-term growth but reducing hydraulic safety margins (Cachinero-Vivar *et al.* 2024). Yet most trait studies stop at the leaf or tree level and seldom connect to ecosystem-scale fluxes, leaving open questions about how structural changes propagate to carbon and water exchange with the atmosphere (Gomarasca *et al.* 2023). Complementary work using eddy-covariance networks has formalized three orthogonal axes of ecosystem function—maximum productivity, water-use strategy, and carbon-use efficiency (Migliavacca *et al.* 2021). Pine forests often lie at the conservative end of the water-use axis, but how thinning shifts their position in this trait space is not well understood (Cachinero-Vivar *et al.* 2024). Linking individual-tree hydraulics to these emergent ecosystem properties would provide a powerful, mechanistic basis for developing adaptive management strategies.

The latest advances in high-resolution imaging spectroscopy demonstrate how trait-based remote sensing can serve as an early-warning system for forest health. In a drought-mortality hotspot of California's Sierra Nevada, Queally *et al.* 2025 recently leveraged NASA AVIRIS-Classic data (15 m, 425 bands) to map foliar nitrogen, lignin, non-structural carbohydrates and leaf mass per area at two NEON sites. Random-forest models combining these traits with soil moisture and topography explained up to 57% of within-pixel tree mortality variance, outperforming models based solely on structural or climatic predictors. Crucially, pre-mortality trait signals (e.g. high LMA, depleted canopy water content) emerged 1–2 years before extensive die-back, confirming that hyperspectral trait maps can reveal latent hydraulic and carbon stresses well ahead of canopy browning. These findings complement airborne and satellite studies that use canopy water content or simple pigment indices as drought

proxies (Asner *et al.* 2015, 2016) yet extend the diagnostic toolkit to a multi-trait physiological space.

While much of this evidence comes from hyperspectral imagers -whose dense spectral sampling is well suited to retrieving water-related traits- achieving similar performance with multispectral sensors remains challenging, particularly for radiative-transfer inversion (Zarco-Tejada *et al.* 2019). Still, PROSAIL inversions can be adapted to multispectral time series (e.g. Sentinel-2/Landsat) to yield continuous canopy-trait estimates relevant to water stress (Zhang and Dietze 2023). Relatedly, Gaussian-process emulators have been used to regularize PROSAIL inversions from multispectral inputs, enabling scalable trait mapping (Estévez *et al.* 2020, 2022). We follow this multispectral route, using Sentinel-2 with explicit uncertainty quantification to track seasonal and treatment-driven shifts in traits linked to canopy water status. Building on that framework, we fuse Sentinel-2 hybrid retrievals (10–20 m) and an uncertainty-aware hybrid inversion to track seasonal and treatment-driven shifts in traits linked to canopy water status, and evaluate their correspondence with ecosystem fluxes. This leverages Sentinel-2's management-scale spatial detail and revisit (Drusch *et al.* 2012) to follow dynamics in key traits (i.e. chlorophyll content CHL, equivalent water thickness EWT, or LMA) relevant to productivity and hydraulics. To our knowledge, such end-to-end integration—linking satellite-derived traits, their uncertainties, and plot-level process measurements—remains rare, and directly addresses the gap in relating canopy traits to ecosystem functioning across management scenarios.

Here we pioneer a unified framework linking tree hydraulics, Sentinel-2-derived biophysical traits, and eddy-covariance fluxes to quantify the eco-physiological consequences of operational thinning in two contrasting pine species. In particular, we focused on the following objectives, to:

- Quantify how moderate-to-heavy thinning alters growth, water-use dynamics, and stem physiological status in two contrasting Mediterranean pine species.
- Assess the relative importance of leaf-level functional traits (Chlorophyll pigments CHL, Leaf Mass Area; LMA, equivalent leaf water thickness; EWT) and stand structure variables (LAI, fAPAR, fractional cover; fCover, albedo) in predicting productivity (GPP), growth (BAI), and stem water dynamics (i.e. maximum daily shrinkage; MDS) across management treatments.
- Determine whether responses to thinning are species specific, reflecting differences in water-use strategy and structural adaptation; and
- Evaluate the potential of radiative transfer modelling to detect and quantify thinning-mediated changes in biochemical and structural properties at both leaf and stand scales.

We hypothesize that:

- Thinning will enhance stand-level water availability and thus increase maximum diurnal stem shrinkage (MDS)—a measure of stem water dynamics—and basal area increment (BAI) in both species, but that the magnitude of these responses will differ by species and,
- Thinning will reduce canopy-scale structural traits (LAI, fAPAR, fCover), leading to declines in GPP, with stand-structure metrics explaining more variance in GPP and MDS, whereas leaf-level traits (LMA, EWT, CHL) will be stronger predictors of BAI.

By integrating measurements from xylem water storage (dendrometry) to canopy biophysics (remote sensing) and ecosystem fluxes (eddy covariance), our study provides a multi-scale basis for optimizing thinning prescriptions to balance growth enhancement with canopy integrity and physiological resilience in Mediterranean pine plantations.

Materials and methods

Study area and sampling design

The study was carried out on the Mairena massif, Sierra Nevada National Park, southern Spain (37.04° N, 3.05° W). This Mediterranean mountain range spans an elevation range between 860–3482 m a.s.l. and experiences cold winters, hot summers, and an average annual precipitation of ∼600 mm, concentrated outside the pronounced dry season (mid-June to mid-September). Mean annual temperatures decline from 12–16°C at foothill elevations to <10°C above 3000 m a.s.l. Natural woodlands (i.e. *Quercus ilex* and *Q. coccifera*) cover ∼20% of the landscape; the remainder is dominated by four non-native pines (*Pinus halepensis*, *P. pinaster*, *P. nigra*, *P. sylvestris*), established during afforestation campaigns in the 1960s–1980s.

A selective-thinning program began in the early 2010s across the plantations. We targeted two high-elevation stands: a *P. sylvestris* forest at 1900–2200 m a.s.l. and a *P. nigra* subsp. salzmannii forest at 1600–1800 m a.s.l. For each species we established paired plots: (i) thinned (T; 50%–70% basal-area removal) and (ii) control (C, no recent intervention). Detailed stand and site characteristics are summarized in Table 1.

Multiscale monitoring of forest structure and functioning

Stem-scale band dendrometers and basal area increment

We quantified short-term stem water dynamics and radial growth using high-precision band-type digital dendrometers (DRL-26C, EMS Brno, CZ). Sensors were mounted at breast height (1.3 m) using stainless-steel bands pre-tensioned according to the manufacturer's specifications. Within each stand (single-cohort plantations established in the 1960s), we selected five dominant or co-dominant pines per stand (20 instrumented trees in total) using a stratified-random protocol designed to minimize potential confounding effects related to tree condition, size, canopy position, and local microsite variability. Eligible trees were required to be free of visible stem or crown damage, to fall within 1–2 standard deviations of the stand mean DBH, and to belong to the dominant or co-dominant canopy class. From this eligible pool, five trees per stand were randomly selected while balancing micro-topographic variation (slope/aspect) where possible. For each tree, we recorded coordinates, DBH, height, and crown class. Site-level slope, aspect, elevation, and pre-thinning stem density were obtained from the forest inventory and were comparable within species.

The devices logged stem-circumference variation (SCV) every 60 min with a resolution of ±1 μm and an intrinsic thermal drift <2 μm °C^{-1}. Following Deslauriers *et al.* 2007, the standardized daily hydrological index of maximum daily shrinkage ($MDS = SCV_{max} - SCV_{min}$) was calculated within each 24-h period, reflecting daytime depletion of internal water stores.

Raw series (2023–2024) were processed with the treenetproc R package (Haeni *et al.* 2020, Knüsel *et al.* 2021). Outliers exceeding ±4 SD were removed (< 0.3% of records). Final SCV and MDS metrics were aggregated to daily and monthly means for subsequent statistical analyses (see Graphical Abstract for workflow overview).

Table 1 Stand and site characteristics for each species and treatments (*P. silvestris* control PSC, *P. sylvestris* thinned PST, *P. nigra* control PNC, *P. nigra* thinned PNT). Stand variables were taken in 15 randomly sampled dominant individuals, resulting in a total of 60 trees (15 × 4 sites) analysed. For each tree, we measured diameter at breast height (DBH, 1.3 m above ground level) using a calliper (Haglöf Mantax, Långsele, Sweden) and total height (H) using a Vertex IV hypsometer (Haglöf, Sweden). We also measured stand density (N, stems ha^{-1}) and basal area (G, m^2 ha^{-1}) for all trees with DBH > 10 cm.

Plot	Lat. (N)	Lon. (W)	Elev. (m a.s.l)	Exp.	Slope (%)	N (trees ha^{-1})	DBH (cm)	H (m)	BA (m^2 ha^{-1})
PSC	37.05	3.05	2024	S	15–25	1160	21.59 (0.35)	11.96 (0.13)	42.47
PST	37.05	3.05	2073	S	35–45	348	25.36 (0.81)	11.17 (0.19)	17.57
PNC	37.04	3.07	1661	SW	15–25	1240	18.30 (0.30)	8.43 (0.13)	32.62
PNT	37.04	3.04	1818	S	15–25	620	20.75 (0.35)	8.55 (0.20)	20.97

Basal area increment (BAI) was reconstructed from tree-ring measurements. In early March 2023 and 2024 we extracted two increment cores per tree at 1.3 m using 5.1 mm Pressler borers, oriented at least 90° apart (n = 15 trees/plot, 60 cores in total). Cores were air-dried, sanded and scanned at 1200 dpi. Ring widths were measured using CooRecorder and cross-dated visually and statistically (COFECHA) to verify dating accuracy (Cachinero-Vivar *et al.* 2024). Ring-width series were converted to BAI and detrended using spline curves with the *dplR* package to remove age- and size-related trends. Stand-level BAI was computed as the mean across trees of each respective stands."

Leaf- and stand-level remote sensing biophysics

A Sentinel-2 PROSAIL–hybrid model was built using a synthetic dataset of biophysical variables generated with the PROSAIL radiative transfer model, which couples the leaf optical model PROSPECT-5 (Feret *et al.* 2008) and the canopy reflectance model 4SAIL (Verhoef 1984). The combined PROSAIL framework simulates top-of-canopy reflectance across the VIS–NIR–SWIR domain as a function of key leaf biochemical parameters (CHL = chlorophyll a + b content (μg cm^{-2}), EWT = equivalent water thickness (cm or its equivalent g cm^{-2}), LMA = leaf dry matter content (g cm^{-2}), and canopy structural parameters (LAI = leaf area index (m^2 m^{-2}), fCover = fractional ground cover (unitless), fAPAR = fraction of absorbed PAR (unitless), and broadband canopy albedo (unitless)). We proceeded as follows:

Forward simulations with PROSAIL radiative transfer model

We sampled each parameter from literature-informed ranges for Mediterranean pines (e.g. CHL 10–80 μg cm^{-2}; EWT 0.005–0.03 g cm^{-2}; LMA 0.005–0.02 g cm^{-2}; LAI 0.5–6 m^2 m^{-2}; fCover 0.2–1.0) using Latin Hypercube Sampling (n = 10 000). We simulated corresponding reflectance spectra at Sentinel-2 band centers (B2–B8A, B11, B12) using the PROSAIL-D model version compiled in the PROSAIL package (Féret and de Boissieu 2024). Each simulated spectrum was paired with its true parameter values to create the Sentinel-2 PROSAIL training library.

Global sensitivity analysis between PROSAIL outputs and Sentinel-2 bands

We quantified the sensitivity of Sentinel-2 reflectance to PROSAIL parameters (CHL, EWT, LMA; and LAI for context) using a global analysis based on Latin-Hypercube sampling of physiologically realistic ranges and the same PROSAIL forward model used in the inversion. For each sample we computed band wise sensitivities with three complementary metrics—standardized regression coefficients (SRC), partial correlations (PCC), and Random-Forest permutation importance—to capture both linear and non-linear effects. The results were physically consistent: CHL was most influential in the red and red-edge (B4–B5), EWT (and, secondarily, LMA) in the SWIR (B11–B12), and LAI in the red-edge/NIR (B6–B8). These diagnostics informed band selection and parameter bounds/priors and guided interpretation of retrieved traits. Soil/background reflectance in PROSAIL was kept at default values and potential background influence was evaluated analytically by including albedo as a covariate in downstream models (Fig. S1, supplementary material).

Inversion via random-Forest in GEE

We imported the PROSAIL library as a feature collection in Google Earth Engine (GEE). For each target trait (LAI, CHL, EWT, LMA, fCover, fAPAR, albedo), we trained a smileRandomForest regressor with 200 trees, using the 10 Sentinel-2 bands as predictors. The Random Forest model was chosen because it handles non-linear relationships and parameter interactions robustly and avoids potential instability in direct physical inversion (Pacheco-Labrador *et al.* 2019).

Mapping Sentinel-2 to biophysical traits

For each monthly median composite of cloud-masked Sentinel-2 scenes within each area of interest (AOI) and year, we applied the seven Random Forest retrieval models to generate per-pixel estimates of leaf and canopy biophysical traits. The resulting predictions were stacked into a seven-band image for each month and spatially averaged within each AOI to obtain plot-scale monthly trajectories. Annual summaries were then derived from these monthly estimates for subsequent analyses (Fig. 1).

Stand-level Eddy covariance flux measurements

We quantified stand-level exchanges of CO_2, water-vapour, and energy above two paired *P. sylvestris* plots —control (PSC) and thinned (PST)— using a paired eddy-covariance (EC) setup (installed March 2024). The sensors were mounted 1.5 m above the canopy height (canopy top = 11 m, measurement height z_m = 12.5 m) so that the upwind fetch did not exceed the coverage area of the respective *P. sylvestris* treatments in all prevailing wind directions in accordance to footprint analysis (Kljun *et al.* 2015) (Fig. 1).

Briefly, the instrumentation setup consisted of a three-dimensional sonic anemometer (Gill R3–50; Gill Instruments Limited, Lymington, UK in PSC and CSAT3, Campbell Scientific, Logan, UT, USA in PST) measuring (u, v, w) components and sonic temperature at 20 Hz. An open-path infrared gas analyser (LI-77500DS in PSC and LI-7500 in PST, LI-COR Biosciences Inc., Lincoln, NE, USA) provided synchronous

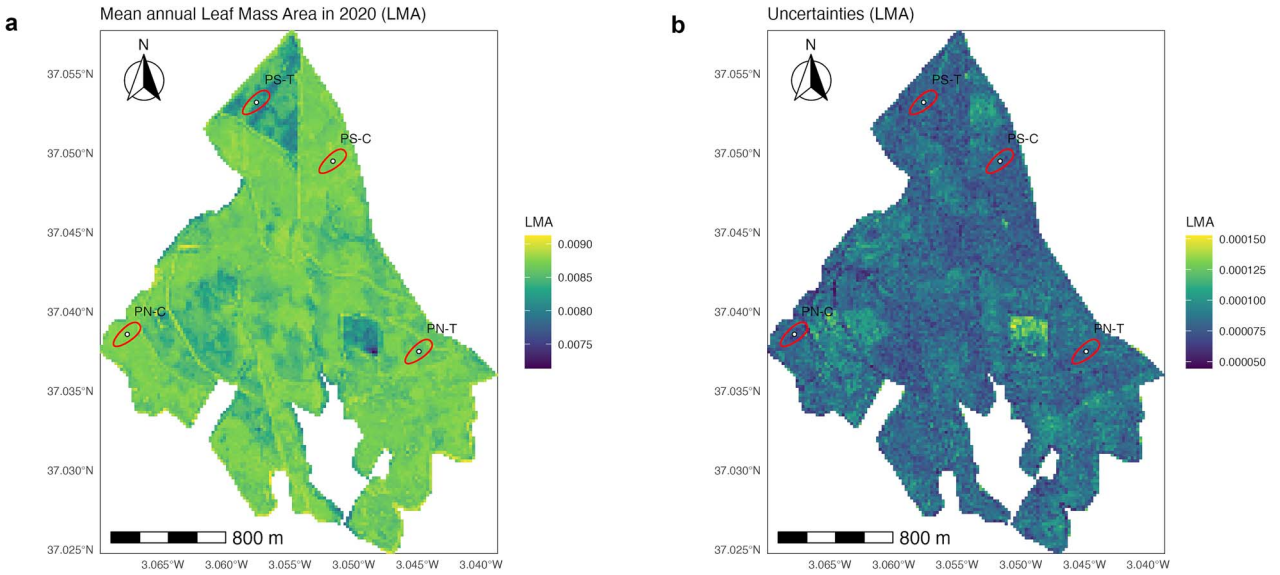

Figure 1 Spatial patterns of leaf mass per area (LMA) and its uncertainty for 2020 at the study site. (a) Mean annual LMA (kg m^{-2}) retrieved from monthly Sentinel-2 composites via PROSAIL inversion and a random-forest ensemble. (b) Uncertainty of LMA expressed as the ensemble standard error (see Methods). Red contours mark the estimated flux footprint for each plot locations (PS-T, PS-C = *Pinus sylvestris* thinned/control; PN-T, PN-C = *P. nigra* thinned/control). North arrow and 800 m scale bar shown; 20 m pixels; non-vegetated areas masked.

CO_2 and H_2O molar densities. Ancillary sensors comprised a four-component net radiometer (CNR4, Kipp & Zonen, Delft, Netherlands), PAR quantum sensor (PQS-1; Kipp & Zonen), and a ventilated temperature/relative-humidity probe (HMP155; Vaisala, FI). Raw 20 Hz data were tilt-corrected, despiked, and time-lag optimized in EddyPro 7.0.9 (LI-COR). Quality control followed (Foken and Wichura 1996) flags 0–1; periods with low friction velocity were discarded. Remaining gaps (< 16% of records) were filled with the (Reichstein *et al.* 2005) marginal distribution approach. A comprehensive description of the data processing steps, error assessment, and quality control procedures is provided in (Perez-Priego *et al.* 2017). Net ecosystem exchange (NEE, μmol CO2 m^{-2} s^{-1}) of CO_2 was separated into gross primary production (GPP, μmol CO_2 m^{-2} s^{-1}) and ecosystem respiration ($R_{ECO,}$ μmol CO_2 m^{-2} s^{-1}) using the night-time method (Reichstein *et al.* 2003, Lasslop *et al.* 2010), implemented in the REddyProc R package (version 0.7–1; (Wutzler *et al.* 2018)).

Statistical analysis

We propagated two sources of uncertainty for the Sentinel-2/PROSAIL trait retrievals: (i) model uncertainty associated with the hybrid inversion, and (ii) stand-scale spatial sampling uncertainty. For each target trait, we trained an ensemble of 20 Random Forest (RF) regressors on a PROSAIL look-up table (Verhoef 1984, Jacquemoud and Baret 1990, Jacquemoud *et al.* 2009), using different random seeds; each RF contained 300 trees. Monthly Sentinel-2 composites were then predicted pixel-wise by all 20 RF models for each trait. For each pixel, we used the ensemble mean as the trait estimate and the ensemble standard deviation as a measure for model-related uncertainty (Breiman 2001).

Stand-level monthly values were computed as the spatial mean of pixel-wise ensemble means within each AOI. Spatial sampling uncertainty was estimated from the standard deviation of these pixel-wise means, converted to a standard error using an effective sample size (n_{eff}) to account for spatial autocorrelation (Dale and Fortin 2014). Specifically, we used

$$SE_{spatial} = SD/\sqrt{n_{eff}} \quad [1]$$

with $n_{eff} = 0.5n$ (minimum 5 pixels). Because plots contained relatively few valid pixels per month, variogram-based estimates of n_{eff} could be unstable, so we adopted this conservative approximation; sensitivity analyses using 0.3n to 0.7n did not alter the conclusions. Model uncertainty in the stand mean was estimated as:

$$SE_{pred} = \frac{\overline{SD_{ens}}}{\sqrt{n}} \quad [2]$$

where $\overline{SD_{ens}}$ is the mean pixel-wise ensemble SD across the AOI. Total retrieval uncertainty was then computed as

$$SE_{total} = \sqrt{SE_{pred}^2 + SE_{spatial}^2} \quad [3]$$

To test thinning effects while accounting for retrieval error, Sentinel-2 traits were propagated through the analysis using a Monte-Carlo errors-in-variables approach (Carroll *et al.* 2006). For each stand-months we drew:

$$x^{(k)} \sim \mathcal{N}\left(\hat{x}, SE_{total}^2\right) \quad [4]$$

where $\hat{x}$is the retrieved stand-month estimate and SE_{total} is the combined uncertainty defined in Eq. (3).

$$x^{(k)} \sim \mathbf{species} \times \mathbf{treatment} + \mathbf{poly}\,(\mathbf{month}, 2) \quad [5]$$

using all months with valid observations. Species-specific treatment contrasts (thinned − control) were then derived from the fitted marginal means. Point estimates and 95% Monte Carlo intervals were obtained from the distribution of these contrasts across all draws. To compare response magnitude across variables, we also reported

Table 2 Overview of all datasets used in the study, listing variable (symbol; units), data source/instrument, spatial unit (stand/tower footprint), site (PSC, PST, PNC, PNT), temporal coverage (years), sampling frequency, number of observations, and the uncertainty metric reported. Sentinel-2/PROSAIL traits include LAI, fCover, fAPAR, LMA, EWT, CHL, and albedo (monthly composites); field data include basal area increment (BAI; core increments), gross primary productivity (GPP; eddy covariance), and mean daily stem variation (MDS; band-dendrometers). For Sentinel-2 traits we report RF-ensemble standard errors aggregated at stand level using the effective sample size. Note that pre-thinning satellite coverage is unavailable for one species, as indicated in the table. Abbreviations: PSC/PST = *P. sylvestris* control/thinned; PNC/PNT = *P. nigra* control/thinned.

Variable	Source	Spatial unit	Stands	Temporal coverage	Frequency
LAI, fCover, fAPAR, albedo, CHL, EWT, LMA	Sentinel-2 → PROSAIL inversion	20 m pixels → stand mean	PSC, PST, PNC, PNT	2016–2025 (monthly composites)	daily → Monthly
BAI	Ring with measurements from increment cores (n = 15 trees/ha)	Tree → stand mean	PSC, PST, PNC, PNT	2010–2014 (specify)	annual summaries
GPP	Eddy covariance	Tower footprint (stand)	PSC, PST	2014–2024 (May–November)	hourly → monthly
SCV/MDS	Dendrometers (n = 5 trees/stand)	Tree → stand mean	PSC, PST, PNC, PNT	2023 (April–August)	hourly → monthly

percent change ($\Delta\% = 100 \times \Delta/\overline{x}$) and standardized effects (Cohen's $d = \Delta/s_p$).

Variables with genuine replications at the tree level (BAI, MDS; n = 15 trees per stand) were analysed with models that respect that replication (ANOVA or linear mixed models with tree as random effect, as appropriate). For GPP (tower-footprint monthly means), treatment effects were summarized as within-species paired-month differences (Thinned–Control) with uncertainty shown as SE of monthly means. Treatment effects were evaluated as within-species monthly contrasts (Thinned − Control), with Sentinel-2/PROSAIL traits analyzed via Monte-Carlo errors-in-variables using RF-ensemble SEs, and GPP/MDS via the same contrast on monthly stand means; species effects were evaluated as *P. sylvestris* − *P. nigra*, with species × treatment interactions reported where informative. All analyses were performed in R version 4.2.2 (R Core Team, 2022).

The Table 2 provides an overview of the dataset used in this study including variables and their respective temporal and spatial coverages.

Model selection and validation

We modelled BAI, GPP, and MDS as functions of Sentinel-2/PROSAIL predictors using ordinary least squares after centering and scaling covariates. Candidate predictors were limited a priori by physiological relevance. To reduce multicollinearity we screened models to ensure VIF < 5 and examined residual diagnostics. Model selection followed stepwise AIC from the full model. Because stepwise procedures can be unstable with correlated predictors, robustness was checked by (i) leave-one-month-out cross-validation of the final model and (ii) ridge-penalized refits; in both checks the leading predictors and effect directions were unchanged. We report adjusted R^2, AIC, and cross-validated RMSE for the final specification.

For variables with tree-level replication (BAI, MDS) we compared treatments using either one-way ANOVA or linear mixed models (tree random effect) after routine checks of assumptions. We inspected residual Q–Q plots and Shapiro–Wilk for normality, and Levene/Brown–Forsythe for equal variances; when variances differed or residuals were non-normal we used Welch's ANOVA or variance-stabilising transforms. For Sentinel-2/PROSAIL traits no ANOVA or Tukey post-hoc tests were applied; all treatment differences derive from the Monte-Carlo errors-in-variables contrasts described above.

Results

Thinning impact on growth and leaf- and stand-level biophysical traits

The annual dynamics of basal-area increment (BAI; $cm^2\ yr^{-1}$) differed between control (PSC, PNC) and thinned (PST, PNT) plots of *Pinus sylvestris* and *Pinus nigra* in response to thinning (Fig. 2). Control plots of both species (PSC and PNC) maintained low and stable BAI values (1–2 $cm^2\ yr^{-1}$), whereas thinned plots (PST and PNT) diverged sharply immediately after treatment (2018 for *P. sylvestris* and 2010 for *P. nigra*). In *P. nigra*, mean BAI in PNT increased from ∼1.5 $cm^2\ yr^{-1}$ pre-thinning to ∼2.7 $cm^2\ yr^{-1}$ in the first three post-thinning years, thereafter plateauing at roughly twice the control level. In *P. sylvestris*, thinning induced an even more pronounced response: mean BAI in PST rose from ∼1.2 $cm^2\ yr^{-1}$ to over 8 $cm^2\ yr^{-1}$ in the two years following treatment, peaking near 10 $cm^2\ yr^{-1}$ in 2020 before a gradual decline toward 6 $cm^2\ yr^{-1}$ by 2024. Vertical error bars represent ±1 SD across trees (n = 15 per plot), and non-overlapping symbols between treatments indicate statistically significant differences (Tukey's HSD, $P < .05$). The contrasting annual BAI dynamics suggest a species-specific growth release upon thinning, with *P. sylvestris* exhibiting a substantially greater and more sustained increase in radial growth than *P. nigra*. This contrast likely reflects that the limiting factors for growth were different between the two species.

Thinning produced modest but statistically supported shifts in leaf-scale traits. In *P. sylvestris*, chlorophyll decreased (ΔCHL = −1.57; 95% CI −1.74, −1.42, Fig. 3a), LMA fell (ΔLMA = −0.000160; −0.000175, −0.000146, Fig. 3c), and leaf water content declined (ΔEWT = −0.000873; −0.000936, −0.000814, Fig. 3e). *In P. nigra*, chlorophyll increased (ΔCHL = +3.65; +3.53, +3.76, Fig. 3a), whereas EWT decreased (ΔEWT = −0.000158; −0.000200, −0.000117) and LMA showed a smaller decline (ΔLMA = −0.0000380; −0.0000450, −0.0000311).

At the canopy scale, structural and radiative metrics showed stronger and consistent thinning effects; LAI decreased in both species (PS: ΔLAI = −0.467; −0.482, −0.453; PN: −0.0679; −0.0779, −0.0580, Fig. 2d), accompanied by reductions in fAPAR (PS: −0.0516;

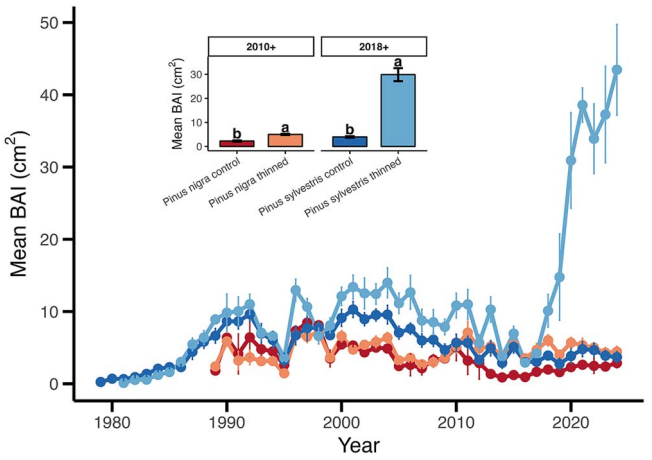

Figure 2 Mean basal-area increment (BAI; cm^2) in four thinning treatments over time. Colored lines with circles show annual mean BAI (± SE) for each treatment: *P. nigra* thinned (PNT, light red), *P. nigra* control (PNC, red), *P. sylvestris* control (PSC, blue) and *P. sylvestris* thinned (PST, light blue). Vertical bars indicate the two analysis periods: '2010' (left; comparison of PNT vs. PNC from 2010 onward) and '2018+' (right; PSC vs. PST from 2018 onward). Bar heights represent mean BAI (± SE) over each period, and superscript letters (a, b) denote groupings from Tukey's HSD test ($\alpha = 0.05$). Thinning substantially increased mean BAI in both species—most notably in *P. sylvestris* (PST) after 2018—while controls maintained low, stable growth.

Table 3 Summary of the three stepwise regression models showing estimated coefficients (β), standard errors (in parentheses), significance levels, sample size (N) and model fit (R^2) for (i) basal area increment (BAI), (ii) gross primary production (GPP), and (iii) maximum daily shrinkage (MDS).

	BAI model	GPP model	MDS model
(Intercept)	16.79	49.66	−11.61
	(152.79)	(22.72)	(72.13)
CHL	3.73***		−0.82*
	(0.88)		(0.35)
EWT	9764.26***	−901.85	
	(1902.55)	(405.60)	
LMA	−87261.47***		
	(16894.68)		
Albedo	1802.82*	−397.06**	774.85
	(721.22)	(112.59)	(494.40)
fAPAR	440.18	64.50*	−247.34
	(224.61)	(26.24)	(124.52)
fCover	−270.50	182.34***	
	(159.14)	(37.00)	
LAI	−60.13**		35.81*
	(19.16)		(13.61)
N	136	14	40
Adjusted R^2	0.61	0.85	0.30

***$P < .001$. **$P < .01$. *$P < .05$.

−0.0539, −0.0495; PN: −0.0308; −0.0324, −0.0293, Fig. 3f). Albedo also declined (PS: −0.00272; −0.00303, −0.00243; PN: −0.00713; −0.00730, −0.00697, Fig. 3b), consistent with greater absorption following canopy opening. Clearly, thinning effects reduced canopy density influencing radiation regime and alteration of the shortwave radiation balance and light interception between treatments.

Overall, magnitudes were small relative to canopy responses, indicating that thinning did alter leaf economics and water status, but stand structure more strongly. The comparative analysis of the magnitude of leaf- vs stand-scale responses showed that stand-scale responses were larger than leaf-scale responses: the median absolute percent change across LAI, fAPAR, fCover and albedo was 6.5%, versus 2.2% for leaf traits (CHL, EWT, LMA) since thinning. Standardized effect sizes (Cohen's d) confirmed that thinning had larger impacts on stand structural traits (median $|d| \approx 0.77$) than on leaf biochemical traits (median $|d| \approx 0.44$). Thus, thinning primarily altered canopy structure and radiative properties, while leaf traits shifted modestly, with the notable exception of a + 9.4% CHL increase in *P. nigra*.

Trait-based models captured a substantial fraction of interannual variation in BAI (Table 3). Leaf-associated traits, particularly LMA, consistently showed the strongest contributions to model performance, while canopy structural traits (LAI, fCover, albedo, fAPAR) provided additional but comparatively less explanatory power. Relative-importance analysis confirmed that leaf traits dominate the explained variance, with LMA emerging as the most influential predictor across Monte-Carlo ensembles.

In practical terms, leaf-level traits emerged as the primary controls on basal area increment (BAI), together explaining 61% of its variance ($R^2 = 0.61$). The strongest predictor was leaf mass per area (LMA): for each 1 g cm^{-2} increase in LMA, BAI declined by 87 261 cm^2 ($\beta = -8.73 \times 10^4$ $cm^2 \cdot [g\ cm^{-2}]^{-1}$, $P < .001$), indicating that heavier, thicker leaves are associated with reduced wood production. Equivalent water thickness (EWT) had the next largest effect, with each 0.01 cm increase in EWT boosting BAI by 98 cm^2 ($\beta = +9764\ cm^2 \cdot cm^{-1}$, $P < .001$), suggesting that greater leaf water content supports stem growth. Chlorophyll content (CHL) also positively influenced BAI ($\beta = +3.73\ cm^2 \cdot (\mu g\ cm^{-2})^{-1}$, $P < .001$), reflecting the role of photosynthetic capacity. Among canopy-level variables, albedo showed a modest positive association with BAI ($\beta = +1802.8\ cm^2$ per unit albedo, $P = .012$), whereas leaf area index (LAI) unexpectedly entered with a small negative coefficient ($\beta = -60.1\ cm^2$ per unit LAI, $P = .002$). Fraction of absorbed PAR (fAPAR; $\beta = +440.2\ cm^2$ per unit, $P = .052$) and fractional cover (fCover; $\beta = -270.5\ cm^2$ per unit, $P = .091$) contributed weakly and were not statistically significant. These results highlight that, under Mediterranean conditions, investments in leaf construction cost (LMA) and water storage (EWT) strongly constrain or promote radial growth, with canopy reflectance (albedo) playing a secondary role.

Drivers of gross primary productivity and stem water dynamic

Gross primary production (GPP) was monitored at the *P. sylvestris* control (PSC) and thinned (PST) sites using a paired eddy-covariance tower setup (Fig. 1). The paired-month contrasts showed that thinning reduced GPP most strongly in spring (May–June), with ΔGPP (Thinned–Control) reaching ∼−9 $\mu mol\ CO_2\ m^{-2}\ s^{-1}$ (Fig. 4a). Reductions were smaller in midsummer (July–August), when the thinned stand assimilated around 3 $\mu mol\ CO_2\ m^{-2}\ s^{-1}$ less than the control. The stronger ΔGPP observed in spring likely reflects the period when reduced competition and improved light conditions after thinning can be most effectively translated into enhanced canopy photosynthesis under still favorable moisture availability. In contrast, during summer, although water depletion becomes more pronounced, increasing drought and atmospheric constraints likely limit the extent to which

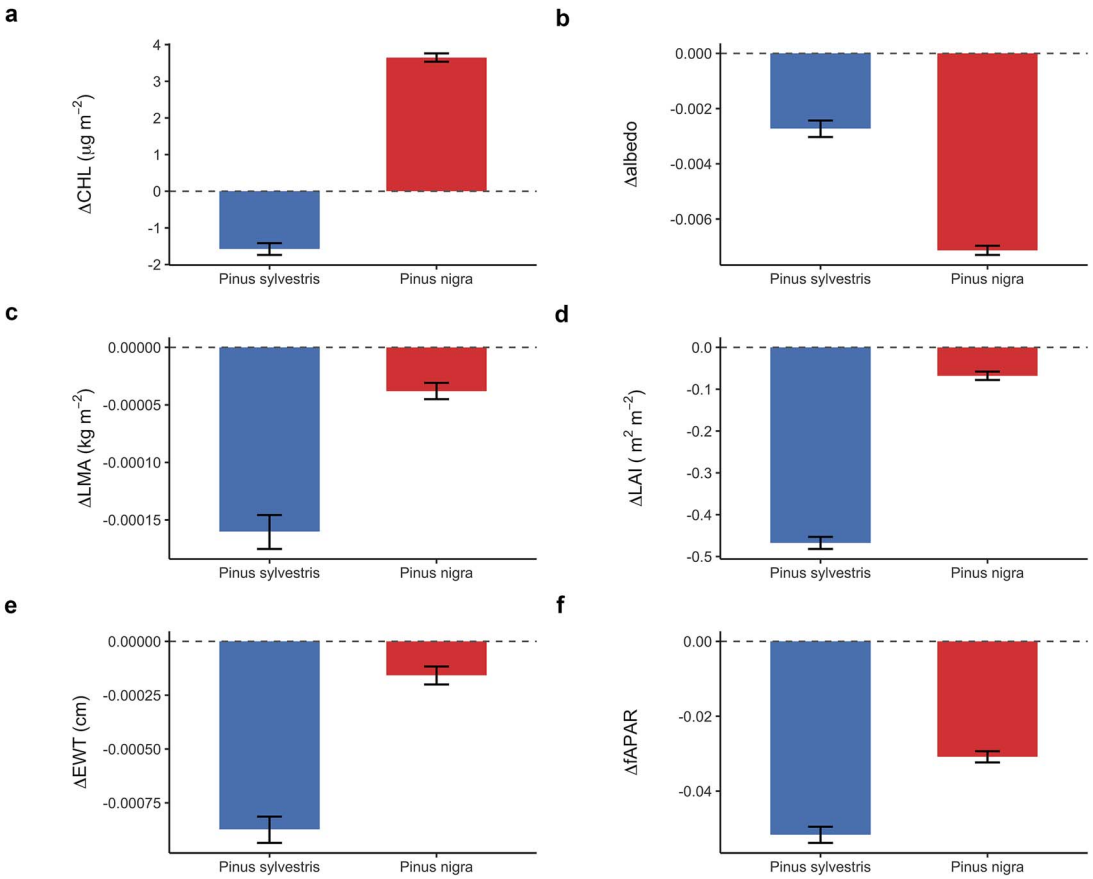

Figure 3 Thinning contrasts for six biophysical traits with propagated retrieval uncertainty. Panels show species-specific mean differences between thinned and control stands for (a) chlorophyll pigment content (CHL), (b) albedo, (c) leaf mass area (LMA), (d) leaf area index (LAI), (e) equivalent water thickness, and (f) fraction of absorbed photosynthetically active radiation fAPAR (units as on y-axes). Bars are species means (blue = *Pinus sylvestris*, red = *P. nigra*); error bars are **95% Monte-Carlo errors-in-variables** intervals from the RF-ensemble SEs; the grey dashed line marks zero (no treatment effect). Negative values indicate reductions after thinning.

this additional resource availability can be converted into higher GPP. Overall, these patterns indicate that thinning curtailed canopy photosynthetic capacity most strongly during the early growing season, with a more moderate effect under peak summer conditions.

Maximum daily stem shrinkage (MDS) responded in the opposite direction—but with a negative ΔMDS (Thinned—Control) in summer, particularly for the case of *P. sylvestris* (Fig. 4b). Note that MDS is determined by negative values as it represents the maximum daily shrinkage of the stem. Therefore, negative ΔMDS is explained by a greater shrinkage of the thinned stand. During July–August, ΔMDS reached nearly around −60 μm, indicating that thinned trees actually exhibited much higher daytime shrinkage than control. Earlier in the year (May–June), when maximum ΔGPP was found, the ΔMDS difference was smaller (∼−20 μm), showing that thinning's impact on hydraulic draw-down was strongest during the driest months.

To uncover which biophysical traits best explained GPP and shrinkage, we regressed both monthly GPP values against Sentinel-2–derived predictors (LAI, fAPAR, fCover, albedo, LMA, EWT, CHL) similar to what we have already described with BAI predictors (Table 3). For the case of GPP (R^2 = 0.85, Table 3, Fig. S2) all retained predictors were stand-scale variables—no leaf-level traits (LMA, CHL) entered the final stepwise model. Fractional cover exerted the strongest positive influence on GPP (β = +182.3 μmol CO_2 m^{-2} s^{-1} per unit fCover, $P < .001$), which translates to an increase of ≈ 18.2 μmol CO_2 m^{-2} s^{-1} for every 0.1 rise in cover. Fraction of absorbed PAR (fAPAR) also boosted GPP (β = +64.5 μmol CO_2 m^{-2} s^{-1} per unit fAPAR, P = .044; ≈ 6.5 μmol per 0.1 change). By contrast, albedo reduced GPP (β = −397.1 μmol CO_2 m^{-2} s^{-1} per unit, P = .004; −39.7 μmol per 0.1), and leaf water content (EWT) had a modest negative effect (β = −901.9 μmol CO_2 m^{-2} s^{-1} per cm, P = .030; −9.0 μmol per 0.01 cm). These results confirm that thinning-driven effects in canopy density and light interception are the primary drivers of reduced GPP in the thinned Scots pine plots, whereas leaf-level physiological traits play a secondary role.

In our multiple-regression model of maximum daily stem shrinkage (MDS), canopy and leaf traits together explained ∼30% of the variance (Table 3, P = .011). Leaf area index (LAI) emerged as the strongest positive driver ($\hat{\beta}$ = + 35.8 μm per unit LAI; P = .013), accounting for roughly 8.4% of the model's explained variance. Chlorophyll content (CHL) was the next most important predictor—contributing ≈ 9.3%—and entered with a small but significant negative effect ($\hat{\beta}$ = − 0.82 μm per μg cm^{-2}; P = .027). The fraction of absorbed PAR (fAPAR) had a marginal negative coefficient ($\hat{\beta}$ = − 247.3 μm per unit fAPAR; P = .055), in line with its 5.0% share of relative importance. Albedo accounted for ∼7.7% of the variance but was not statistically significant ($\hat{\beta}$ = + 774.8 μm per unit albedo; P = .13). Together, these results indicate that thinning drives greater diurnal stem-water draw-down, particularly for *P. sylvestris*, while leaf-level pigment traits modulate shrinkage to a lesser extent.

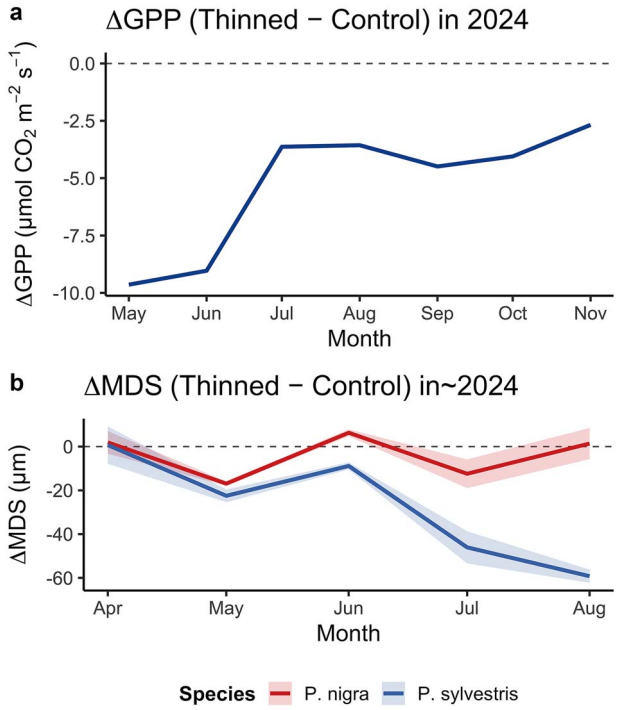

Figure 4 Monthly differences between thinned and control plots in 2024, expressed as 'thinned – control.' (a) ΔGPP (μmol CO_2 m^{-2} s^{-1}), showing consistently negative values from May through September, indicating that thinning reduced stand-scale GPP by ∼9 μmol CO_2 m^{-2} s^{-1} in early summer and ∼4 μmol CO_2 m^{-2} s^{-1} by autumn. (b) ΔMDS (mean daily shrinkage; μm) for both species: *P. nigra* (red) and *P. sylvestris* (blue). The ribbons represent **tree-to-tree variability** within each species and month, computed as the standard deviation of daily ΔMDS across individual trees. MDS values are negative by definition (daily radial contraction relative to morning radius); larger negative values correspond to greater stem shrinkage. Therefore, negative ΔMDS values in May–August indicates that thinned plots experienced higher diurnal stem-shrinkage cycles (i.e. greater hydraulic drawdown) compared to controls, with *P. sylvestris* showing the greatest buffering effect (ΔMDS down to −115 μm in August). The dashed horizontal line at zero marks no change. Note that MDS represents a reduction in stem dimension and it denotes negative values.

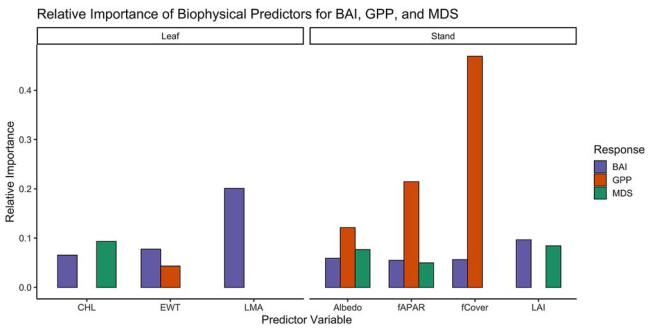

Figure 5 Relative importance of biophysical predictors for basal area increment (BAI), gross primary production (GPP), and maximum daily stem shrinkage (MDS) grouped by trait category. Bars show the proportion of explained variance attributable to each predictor (calculated via the 'lmg' metric in the relaimpo package) for (i) leaf-level optical traits—chlorophyll content (chl), equivalent water thickness (ewt), and leaf mass per area (lma)—and (ii) stand-scale structural and radiative traits—albedo, fraction of absorbed PAR (fAPAR), fractional cover (fCover), and leaf area index (LAI). Colors indicate the response variable: BAI (blue), GPP (orange), and MDS (green). Leaf-level LMA dominates BAI prediction, whereas canopy structural metrics, especially fCover (≈ 47%) and fAPAR (≈ 21%), govern GPP. Hydraulic draw-down (MDS) is jointly influenced by leaf chlorophyll (∼9%), LAI (∼8%), and radiative traits (albedo ∼8%, fAPAR ∼5%), highlighting the hierarchical control of biophysical properties across scales.

In summary, our relative-importance analysis reveals a clear divergence regarding which biophysical traits drive different ecosystem functions (Fig. 5). Tree growth (BAI) was most strongly tied to leaf-level structure: leaf mass per area (LMA) alone explained ∼20% of the variance, with canopy structural and physiological traits (LAI, EWT, CHL) each contributing roughly 6–10%, and the remaining variables (albedo, fAPAR, fCover) adding 5–6% apiece. In contrast, gross primary production (GPP) was dominated by stand-scale light interception: fractional cover accounted for nearly half (≈ 47%) of the explained variance, followed by fAPAR (≈ 21%) and albedo (≈ 12%), while leaf water content (EWT) made only a small contribution (≈ 4%) and other leaf traits were negligible. Hydraulic dynamics (mean daily shrinkage, MDS) fell between these extremes: leaf chlorophyll content was the top predictor (≈ 9%), closely followed by LAI (≈ 8%), albedo (≈ 8%), and fAPAR (≈ 5%). Together, these patterns underscore that growth, productivity, and water-use dynamics in Mediterranean pine stands are each controlled by distinct combinations of leaf- and canopy-level biophysical properties.

Discussion

Our multi-scale analysis shows that thinning-induced differences in canopy and foliar properties are reflected in distinct RTM-derived biophysical traits, which are in turn differently associated with growth, productivity, and water-use dynamics. Basal area increment (BAI) was predominantly associated with leaf-level structure (LMA), whereas gross primary production (GPP) was more strongly related to stand-scale light interception (fCover, fAPAR). Mean daily shrinkage (MDS), in contrast, was best explained by a combination of pigment-related and canopy structural traits (CHL, LAI, albedo). These results highlight that no single trait axis capture all ecosystem responses to management: rather, different structural and physiological dimensions of canopy functioning appear to underlie variations in wood growth, carbon assimilation, and hydraulic stress.

Biophysical constraints of stem radial growth

Thinning reduced GPP while nearly doubling radial growth in *P. sylvestris* (Fig. 2, Fig. 3a), yet it also intensified maximum daily stem-shrinkage cycles (MDS, Fig. 3b), indicating a shift toward faster water turnover. This behaviour is consistent with experiments in Scots pine, where lower stand density enhanced stomatal conductance and midday transpiration but at the cost of greater stem water drawdown (Whitehead *et al.* 1984, Meinzer *et al.* 2001). By contrast, the conservative *P. nigra* displayed only moderate growth gains (Fig. 2) and negligible changes in stem-water dynamics (Fig. 3b), echoing previous reports of limited hydraulic plasticity and higher intrinsic water-use efficiency in this species (Skubel *et al.* 2015).

Trait-based models captured a substantial fraction of interannual variation in BAI (Table 3, Fig. S2). Leaf-associated traits—particularly LMA—consistently showed the strongest contributions to model performance, whereas structural canopy traits (LAI, fCover, albedo, fAPAR) provided additional but comparatively smaller explanatory power. Relative-importance analysis confirmed that leaf traits

dominate the explained variance, with LMA emerging as the most influential predictor across Monte-Carlo ensembles.

The importance of leaf-level traits in explaining growth variation aligns with previous evidence that LMA integrates long-term adjustments in carbon allocation and sclerophylly (Rosas *et al.* 2019, Cachinero-Vivar *et al.* 2024). Therefore, LMA is presented as a primary regulator of radial growth responses to thinning. In our multiple-regression framework, LMA emerged as the single most important predictor, and carried a significant negative coefficient, meaning that treatments which drove LMA downward (thinning) consistently produced larger basal-area increments.

The observed inverse relationship between LMA and BAI aligns with Cachinero-Vivar *et al.* (2024), who found that lower LMA corresponds to improved hydraulic status and greater photosynthetic performance, indicating that thinning-induced reductions in LMA can facilitate higher stem-growth. Taken together, these findings place LMA within a broader hierarchy of trait controls on forest functioning: canopy structure—summarized by LAI and fCover—governs light interception and within-canopy irradiance; leaf water content (EWT) reflects plant water status under prevailing soil–atmosphere demand; and intrinsic leaf construction costs (LMA) constrain growth potential. This hierarchy is consistent with the leaf-economics and canopy-radiation literature.

For example, the worldwide leaf economics spectrum shows that low-LMA leaves invest less in structural tissue and turn over more rapidly, allowing higher relative-growth rates across species (Wright *et al.* 2004). Poorter *et al.* (2009) found that LMA alone explained up to 50% of interspecific variation in relative growth rate, even when controlling for light environment. At the same time, canopy-level traits like LAI and fAPAR have long been recognized as the primary controls on stand-scale carbon assimilation (Niinemets and Valladares 2006), and leaf water content modulates stomatal conductance and photosynthetic capacity under water stress (Olson *et al.* 2014). Together, these studies confirm that although stand density and canopy water status set the upper bound on resource supply, it is the leaf-level cost–benefit trade-off embodied in LMA that dictates how much of those resources can be converted into new wood.

Biophysical constraints of gross primary productivity

At the ecosystem scale, gross primary production was overwhelmingly controlled by fractional cover (≈47% of explained variance), with fAPAR (≈21%) and albedo (≈12%) also playing major roles (Fig. 5). This dominance of canopy-scale light interception metrics over leaf-level physiology underscores that, in water-limited Mediterranean forests, thinning's principal effect on carbon uptake arises through alterations in canopy density rather than changes in foliar chemistry or water content. The small contribution of leaf-level EWT (≈4%) further confirms that instantaneous water status is less limiting for stand-level carbon assimilation than the total leaf area and its light-absorbing capacity.

This pattern finds strong support in both theoretical and empirical ecosystem-scale studies. The classic light-use efficiency framework of Monteith (1972) demonstrates that GPP is fundamentally proportional to the product of absorbed radiation (fAPAR·PAR) and an efficiency term (ε), immediately elevating canopy-scale fAPAR (and by extension fractional cover) to primary constraints of carbon uptake. Empirical syntheses from eddy covariance global FLUXNET analyses show that variations in fAPAR and leaf area index explain more than half of the interannual variability in GPP, while leaf-level biochemical traits (e.g. nitrogen or water content) contribute far less once canopy structure is accounted for (Running *et al.* 1999, Ustin and Gamon 2010). In Mediterranean woodlands, Vogt *et al.* (1986) found that seasonal changes in canopy density drove 70–80% of GPP fluctuations, whereas leaf water potential and chlorophyll concentration had only minor effects under moderate drought. Similarly, Croft *et al.* (2015) reported that manipulations of LAI produced proportional shifts in eddy-covariance GPP, reinforcing that overall leaf area swamps instantaneous physiological status as the key control on ecosystem-scale photosynthesis. The minimal role of EWT in our analysis (∼4%) aligns with these findings, suggesting that, at the monthly timescale and under moderate water limitation, the supply of photosynthetic surface and light interception capacity overwhelmingly governs carbon assimilation in this Mediterranean environment.

To further assess whether thinning modified canopy light-use functioning, we explored the interaction between fAPAR and treatment on monthly GPP. While GPP remained significantly related to fAPAR, the interaction was not significant, suggesting that thinning did not substantially alter the fAPAR–GPP relationship. In this context, the lower stand-level GPP observed in thinned plots appears to be mainly driven by reduced canopy light interception, whereas the enhanced individual-tree growth likely reflects post-thinning shifts in resource availability and allocation rather than increased carbon gain efficiency per unit of absorbed radiation.

Biophysical constraints of stem water dynamics

Maximum daily stem shrinkage—a proxy for daytime hydraulic drawdown—was jointly shaped by leaf chlorophyll content (≈9%), LAI (≈8%), albedo (≈8%), and fAPAR (≈5%, Fig. 5). Thinning boosted overall shrinkage (negative ΔMDS) during the hottest months, indicating that sparser canopies boosted tree-level transpiration demand. The outsized influence of pigment density (CHL) suggests that foliage biochemical adjustments (e.g. reduced chlorophyll loading) can modulate hydraulic safety margins, while canopy architecture continues to dictate the bulk of diurnal water-use patterns.

This hierarchy of controls on daily hydraulic draw-down finds strong support in the stem-dendrometer literature and ecohydrological theory. Dendrometer studies (Zweifel *et al.* 2006, Deslauriers *et al.* 2007) have long shown that canopy transpiration demand, rather than soil-root supply alone, drives the magnitude of daily maximum stem shrinkage (MDS). On the other hand, our finding that pigment density (CHL) explains ∼9% of MDS variance is aligned with Asner *et al.* (2016), who demonstrated that lower canopy chlorophyll—and thus reduced photosynthetic capacity—corresponds with smaller diurnal water-loss cycles under drought, likely through down-regulation of stomatal conductance. Meanwhile, LAI and albedo each account for ∼8% of the variance, confirming that canopy architecture sets the envelope of transpiration demand by modulating intercepted radiation and boundary-layer conductance (Niinemets and Valladares 2006). The ∼5% contribution of fAPAR further underlines that the fraction of absorbed PAR scales with stomatal opening and thus daily water use (Gamon and Surfus 1999). Finally, the negative ΔMDS in thinned stands—particularly during the hottest months—aligns with classic spacing experiments in pines (del Campo *et al.* 2022) which have shown that lower stand density increases overall tree transpiration. Together, these lines of evidence confirm that while canopy structure governs the bulk of diurnal water-use patterns, leaf-level pigment

adjustments fine-tune hydraulic safety margins under changing light and water availability.

In summary, these findings reveal that silvicultural treatments reshape ecosystem function through trait-specific pathways: canopy architecture drives carbon fluxes and water-use dynamics, whereas leaf-level structure governs long-term growth. Recognizing this multi-trait control is essential for designing thinning regimes that optimize wood production, carbon sequestration, and hydraulic resilience to Mediterranean drought.

Limitations and future prospects of radiative-transfer trait retrieval

Despite its demonstrated utility, radiative-transfer inversion for canopy trait mapping yet carries several important caveats that forest managers should consider. First, PROSAIL-based retrievals assume a homogeneous, turbid-medium canopy and often neglect structural complexities such as leaf clumping, understory reflectance and branch-wood scattering, which can introduce bias in heterogeneous stands or mixed-species plantations. Second, Sentinel-2's multispectral bands, while temporally dense, lack the fine spectral resolution of airborne imaging spectrometers, limiting accurate separation of tightly correlated traits (e.g. LMA vs. leaf dry-matter content) and reducing sensitivity under extreme stress. Third, inversion accuracy depends critically on the realism of the training simulation (e.g. choice of prior distributions, soil reflectance and observation geometry), meaning that site-specific calibration and field validation remain essential—particularly when applying models across different bioclimatic zones or management regimes.

In addition, hybrid PROSAIL–RF retrievals carry non-negligible prediction uncertainty arising from model structural errors, spectral noise and the limited representativeness of the training library. In our study, we explicitly propagated monthly retrieval uncertainty into all thinning contrasts and trait–function regressions, yet some degree of attenuation of effect sizes—particularly for LAI and chlorophyll—cannot be excluded. These uncertainties should therefore be considered when using trait retrievals for operational monitoring or decision-support, where confidence intervals remain crucial for interpreting temporal trends and treatment effects.

Nonetheless, by coupling PROSAIL-derived trait time series with independent measurements of growth, carbon fluxes and hydraulics, our results demonstrate that radiative-transfer approaches can reliably detect thinning-mediated changes in canopy biochemistry and structure at both leaf and stand scales—representing a substantive step forward toward operational, trait-based forest monitoring despite these inherent limitations. Future advances in model complexity (e.g. 3-D canopy architecture, background and shadow components; Zarco-Tejada *et al.* 2019, fusion with LiDAR, and the advent of global hyperspectral missions (EnMAP, CHIME, SBG)) promise to further enhance the precision and applicability of trait-based remote sensing for adaptive silviculture and climate-smart forest planning.

Conclusions

Our integrated analysis across canopy biophysics, stem hydraulics, and ecosystem fluxes reveals that thinning in Mediterranean pine plantations exerts distinct, trait-specific controls on growth, productivity, and water-use dynamics. Tree-level radial increment (BAI) is driven primarily by leaf-level construction costs (LMA), whereas ecosystem-scale gross primary production (GPP) depends overwhelmingly on canopy light interception (fractional cover and fAPAR). Maximum daily shrinkage (MDS) sits between these extremes, reflecting a balance of pigment density (CHL) and canopy architecture (LAI, albedo, fAPAR). By partitioning the relative importance of these traits, we demonstrate that no single biophysical axis can predict all ecosystem responses to silvicultural treatments.

Our work further shows that hybrid PROSAIL–Random Forest inversion of Sentinel-2 imagery, when calibrated and validated against in situ growth and flux measurements, provides a powerful tool for operational monitoring of thinning outcomes. Although inversion approaches carry well-documented limitations (canopy heterogeneity, spectral resolution, training realism), coupling remotely sensed trait time series with dendrometer and eddy-covariance data enables early detection and quantification of management-mediated changes at scales relevant to forestry practice.

Overall, these findings underscore the value of a multi-trait, multi-scale monitoring framework to enable climate-adaptive forest management. By targeting specific combinations of leaf and canopy properties, practitioners can design thinning regimes that optimize wood production, maintain carbon sequestration capacity, and bolster hydraulic resilience to Mediterranean drought. Future work should extend this approach to mixed-species stands, integrate emerging hyperspectral data, and explore dynamic feedbacks between management, disturbance, and ecosystem function.

Acknowledgements

Special thanks go to Enrique Echevarría-Martín and Esther Cardell for their support during the field installation and infographic design. We thank the anonymous reviewers for their thoughtful and constructive comments, which substantially improved the clarity and rigor of this manuscript. We are also grateful to Pablo Zarco-Tejada for constructive input on the manuscript draft.

Author contributions

Antonio M Cachinero-Vivar (Conceptualization, Data curation, Formal analysis, Investigation, Methodology, Software, Writing—original draft, Writing—review & editing), Enrique Sánchez-Cañete (Conceptualization, Investigation, Methodology, Resources, Writing—review & editing), Andrew S Kowalski (Conceptualization, Funding acquisition, Methodology, Resources, Supervision, Writing—review & editing), and Óscar Pérez-Priego (Conceptualization, Data curation, Formal analysis, Funding acquisition, Investigation, Methodology, Project administration, Resources, Software, Supervision, Validation, Visualization, Writing—original draft)

Supplementary material

Supplementary material are available at *Forestry* online.

Conflicts of interest

The authors declare that they have no known competing financial interests or personal relationships that could have appeared to influence the work reported in this paper.

Funding

This work was supported by the following projects: The Ministry of Science, Innovation and Universities (REMEDIO PID2021-128463OB-I00), (EVIDENCE 2822/2021) and (Next Generation BIOD22_00033_17_PPCB).

Data availability

The data that support the findings of this study are available from the corresponding author upon reasonable request.

References

Asner, G.P., Brodrick, P.G., Anderson, C.B., *et al.* 2016 Progressive forest canopy water loss during the 2012-2015 California drought. *Proc Natl Acad Sci U S A* **113**, E249–E255. https://doi.org/10.1073/pnas.1523397113.

Asner, G.P., Martin, R.E., Anderson, C.B., *et al.* 2015 Quantifying forest canopy traits: imaging spectroscopy versus field survey. *Remote Sens Environ* **158**, 15–27. https://doi.org/10.1016/j.rse.2014.11.011.

Breiman, L. 2001 Random forests. *Machine learning* **45**, 5–32. https://doi.org/10.1023/A:1010933404324.

Cachinero-Vivar, A.M., Navarro-Cerrillo, R.M., Cabrera-Puerto, R.J., *et al.* 2024 Impact of thinning on leaf economics, plant hydraulics, and growth dynamics. *For Ecol Manage* **562**, 121914. https://doi.org/10.1016/j.foreco.2024.121914.

del Campo, A.D., Otsuki, K., Serengil, Y., *et al.* 2022 A global synthesis on the effects of thinning on hydrological processes: Implications for forest management. In *Forest Ecology and Management*. Vol. **519**. Elsevier B.V. doi:https://doi.org/10.1016/j.foreco.2022.120324, p. 120324.

Carroll, R.J., Ruppert, D., Stefanski, L.A., *et al.* 2006 *Measurement Error in Nonlinear Models: A Modern Perspective*. Chapman and Hall/CRC, https://doi.org/10.1201/9781420010138.

Cramer, W., Bondeau, A., Woodward, F.I., *et al.* 2001 Global response of terrestrial ecosystem structure and function to CO2 and climate change: results from six dynamic global vegetation models. *Glob Chang Biol* **7**, 357–373. https://doi.org/10.1046/j.1365-2486.2001.00383.x.

Croft, H., Chen, J.M., Froelich, N.J., *et al.* 2015 Seasonal controls of canopy chlorophyll content on forest carbon uptake: implications for GPP modeling. *J Geophys Res Biogeo* **120**, 1576–1586. https://doi.org/10.1002/2015JG002980.

Dale, M.R.T. and Fortin, M.-J. 2014 *Spatial Analysis: A Guide for Ecologists*. Cambridge University Press, Cambridge, https://doi.org/10.1017/CBO9780511978913.

Davi, H., Baret, F., Huc, R., *et al.* 2008 Effect of thinning on LAI variance in heterogeneous forests. *For Ecol Manage* **256**, 890–899. https://doi.org/10.1016/j.foreco.2008.05.047.

Deslauriers, A., Rossi, S. and Anfodillo, T. 2007 Dendrometer and intra-annual tree growth: what kind of information can be inferred? *Dendrochronologia* **25**, 113–124. https://doi.org/10.1016/j.dendro.2007.05.003.

Drusch, M., Del Bello, U., Carlier, S., *et al.* 2012 Sentinel-2: ESA's optical high-resolution Mission for GMES operational services. *Remote Sens Environ* **120**, 25–36. https://doi.org/10.1016/j.rse.2011.11.026.

Estévez, J., Salinero-Delgado, M., Berger, K., *et al.* 2022 Gaussian processes retrieval of crop traits in Google earth engine based on Sentinel-2 top-of-atmosphere data. *Remote Sens Environ* **273**, 112958. https://doi.org/10.1016/j.rse.2022.112958.

Estévez, J., Vicent, J., Rivera-Caicedo, J.P., *et al.* 2020 Gaussian processes retrieval of LAI from Sentinel-2 top-of-atmosphere radiance data. *ISPRS Journal of Photogrammetry and Remote Sensing* **167**, 289–304. https://doi.org/10.1016/j.isprsjprs.2020.07.004.

Féret, J.-B. and de Boissieu, F. 2024 Prospect: an R package to link leaf optical properties with their chemical and structural properties with the leaf model PROSPECT. *Journal of Open Source Software* **9**, 6027. https://doi.org/10.21105/joss.06027.

Feret, J.B., François, C., Asner, G.P., *et al.* 2008 PROSPECT-4 and 5: advances in the leaf optical properties model separating photosynthetic pigments. *Remote Sens Environ* **112**, 3030–3043. https://doi.org/10.1016/j.rse.2008.02.012.

Foken, T. and Wichura, B. 1996 Agricultural and forest meteorology tools for quality assessment of surface-based flux measurements. In *Agricultural and Forest Meteorology*. Vol. **78**, pp. 83–105. https://doi.org/10.1016/0168-1923(95)02248-1.

Gamon, J.A. and Surfus, J.S. 1999 Assessing leaf pigment content and activity with a reflectometer. *New Phytol* **143**, 105–117. https://doi.org/10.1046/j.1469-8137.1999.00424.x.

Gomarasca, U., Migliavacca, M., Kattge, J., *et al.* 2023 Leaf-level coordination principles propagate to the ecosystem scale. *Nature. Communications* **14**, 3948. https://doi.org/10.1038/s41467-023-39572-5.

Haeni M, Knüsel S, Peters RL. *et al.* Treenetproc–clean, process and visualise dendrometer data. 2020. *R Package Version 0.1*, *4*.

Jacquemoud, S. and Baret, F. 1990 PROSPECT: a model of leaf optical properties spectra. *Remote Sens Environ* **34**, 75–91. https://doi.org/10.1016/0034-4257(90)90100-Z.

Jacquemoud, S., Verhoef, W., Baret, F., *et al.* 2009 PROSPECT+ SAIL models: a review of use for vegetation characterization. *Remote Sens Environ* **113**, S56–S66. https://doi.org/10.1016/j.rse.2008.01.026.

Kljun, N., Calanca, P., Rotach, M.W., *et al.* 2015 A simple two-dimensional parameterisation for flux footprint prediction (FFP). *Geosci Model Dev* **8**, 3695–3713. https://doi.org/10.5194/gmd-8-3695-2015.

Knüsel, S., Peters, R.L., Haeni, M., *et al.* 2021 Processing and extraction of seasonal tree physiological parameters from stem radius time series. *Forests* **12**, 765. https://doi.org/10.3390/f12060765.

Lasslop, G., Reichstein, M., Papale, D., *et al.* 2010 Separation of net ecosystem exchange into assimilation and respiration using a light response curve approach: critical issues and global evaluation. *Glob Chang Biol* **16**, 187–208. https://doi.org/10.1111/j.1365-2486.2009.02041.x.

Manning, P., Van Der Plas, F., Soliveres, S., *et al.* 2018 Redefining ecosystem multifunctionality. In *Nature Ecology and Evolution*. Vol. **2**. Nature Publishing Group, pp. 427–436. https://doi.org/10.1038/s41559-017-0461-7.

Meinzer, F.C., Goldstein, G. and Andrade, J.L. 2001 Regulation of water flux through tropical forest canopy trees: do universal rules apply? *Tree Physiol* **21**, 19–26. https://doi.org/10.1093/treephys/21.1.19.

Migliavacca, M., Musavi, T., Mahecha, M.D., *et al.* 2021 The three major axes of terrestrial ecosystem function. *Nature* **598**, 468–472. https://doi.org/10.1038/s41586-021-03939-9.

Monteith, J.L. 1972 Solar radiation and productivity in tropical ecosystems. *J Appl Ecol* **9**, 747–766.

Niinemets, Ü. and Valladares, F. 2006 Tolerance to shade, drought, and waterlogging of temperate northern hemisphere trees and shrubs. *Ecological monographs* **76**, 521–547. https://doi.org/10.1890/0012-9615(2006)076[0521:TTSDAW]2.0.CO;2.

Olson, M.E., Anfodillo, T., Rosell, J.A., *et al.* 2014 Universal hydraulics of the flowering plants: vessel diameter scales with stem length across angiosperm lineages, habits and climates. *Ecol Lett* **17**, 988–997. https://doi.org/10.1111/ele.12302.

Pacheco-Labrador, J., Perez-Priego, O., El-Madany, T.S., *et al.* 2019 Multiple-constraint inversion of SCOPE. Evaluating the potential of GPP and SIF for the retrieval of plant functional traits. *Remote Sens Environ* **234**, 111362. https://doi.org/10.1016/j.rse.2019.111362.

Perez-Priego, O., El-Madany, T.S., Migliavaca, M., *et al.* 2017 Evaluation of eddy covariance latent heat fluxes with independent lysimeter and sapflow estimates in a Mediterranean savannah ecosystem. *Agric For Meteorol* **236**, 87–99. https://doi.org/10.1016/j.agrformet.2017.01.009.

Poorter, H., Niinemets, Ü., Poorter, L., *et al.* 2009 Causes and consequences of variation in leaf mass per area (LMA): A meta-analysis. In *New Phytologist*. Vol. **182**, pp. 565–588. https://doi.org/10.1111/j.1469-8137.2009.02830.x.

Queally, N., Zheng, T., Ye, Z., *et al.* 2025 Functional traits from imaging spectroscopy inform patterns of Forest mortality during Sierra Nevada drought. *Glob Chang Biol* **31**, e70246. https://doi.org/10.1111/gcb.70246.

Reichstein, M., Falge, E., Baldocchi, D., *et al.* 2005 On the separation of net ecosystem exchange into assimilation and ecosystem respiration: Review and improved algorithm. In *Global Change Biology*. Vol. **11**, pp. 1424–1439. https://doi.org/10.1111/j.1365-2486.2005.001002.x.

Reichstein, M., Tenhunen, J., Roupsard, O., *et al.* 2003 Inverse modeling of seasonal drought effects on canopy CO2/H2O exchange in three Mediterranean ecosystems. *J Geophys Res Atmos* **108**. https://doi.org/10.1029/2003jd003430.

Rosas, T., Mencuccini, M., Barba, J., *et al.* 2019 Adjustments and coordination of hydraulic, leaf and stem traits along a water availability gradient. *New Phytol* **223**, 632–646. https://doi.org/10.1111/nph.15684.

Running SW, Baldocchi DD, Turner DP. *et al.* (1999). A Global Terrestrial Monitoring Network Integrating Tower Fluxes, Flask Sampling, Ecosystem Modeling and EOS Satellite Data. http://www-eosdis.

Rustad, L.E. 2008 The response of terrestrial ecosystems to global climate change: towards an integrated approach. *Sci Total Environ* **404**, 222–235. https://doi.org/10.1016/j.scitotenv.2008.04.050.

Silva, L.C.R. and Lambers, H. 2021 Soil-plant-atmosphere interactions: Structure, function, and predictive scaling for climate change mitigation. In *Plant and Soil*. Vol. **461**. Springer Science and Business Media Deutschland GmbH, pp. 5–27. https://doi.org/10.1007/s11104-020-04427-1.

Skubel, R., Arain, M.A., Peichl, M., *et al.* 2015 Age effects on the water-use efficiency and water-use dynamics of temperate pine plantation forests. *Hydrol Process* **29**, 4100–4113. https://doi.org/10.1002/hyp.10549.

Sohn, J.A., Saha, S. and Bauhus, J. 2016 Potential of forest thinning to mitigate drought stress: a meta-analysis. *For Ecol Manage* **380**, 261–273. https://doi.org/10.1016/j.foreco.2016.07.046.

Team, R. C 2022 *R: A Language and Environment for Statistical Computing and Graphics*. Foundation for Statistical Computing.

Ustin, S.L. and Gamon, J.A. 2010 Remote sensing of plant functional types. In *New Phytologist*. Vol. **186**, pp. 795–816. https://doi.org/10.1111/j.1469-8137.2010.03284.x.

Vadell, E., De-Miguel, S. and Pemán, J. 2016 Large-scale reforestation and afforestation policy in Spain: a historical review of its underlying ecological, socioeconomic and political dynamics. *Land Use Policy* **55**, 37–48. https://doi.org/10.1016/j.landusepol.2016.03.017.

Verhoef, W. 1984 Light scattering by leaf layers with application to canopy reflectance modeling: the SAIL model. *Remote Sens Environ* **16**, 125–141. https://doi.org/10.1016/0034-4257(84)90057-9.

Vogt, K.A., Grier, C.C. and Vogt, D.J. 1986 Production, turnover, and nutrient dynamics of above-and belowground detritus of world forests. In *Advances in Ecological Research*. Vol. **15**. Elsevier, pp. 303–377. https://doi.org/10.1016/S0065-2504(08)60122-1.

Whitehead, D., Jarvis, P.G. and Waring, R.H. 1984 Stomatal conductance, transpiration, and resistance to water uptake in a Pinus sylvestris spacing experiment. *Can J For Res* **14**, 692–700. https://doi.org/10.1139/x84-124.

Wright IJ, Reich PB, Westoby M. *et al.* (2004). The worldwide leaf economics spectrum. www.nature.com/nature

Wutzler, T., Lucas-Moffat, A., Migliavacca, M., *et al.* 2018 Basic and extensible post-processing of eddy covariance flux data with REddyProc. *Biogeosciences* **15**, 5015–5030. https://doi.org/10.5194/bg-15-5015-2018.

Zarco-Tejada, P.J., Hornero, A., Beck, P.S.A., *et al.* 2019 Chlorophyll content estimation in an open-canopy conifer forest with sentinel-2A and hyperspectral imagery in the context of forest decline. *Remote Sens Environ* **223**, 320–335. https://doi.org/10.1016/j.rse.2019.01.031.

Zhang, D. and Dietze, M. 2023 Towards uninterrupted canopy-trait time-series: a Bayesian radiative transfer model inversion using multi-sourced satellite observations. *Remote Sens Environ* **287**, 113475. https://doi.org/10.1016/j.rse.2023.113475.

Zweifel, R., Zimmermann, L., Zeugin, F., *et al.* 2006 Intra-annual radial growth and water relations of trees: implications towards a growth mechanism. *J Exp Bot* **57**, 1445–1459. 562. https://doi.org/10.1093/jxb/erj125.

Forestry: An International Journal of Forest Research, 2026, **99**, cpag041
https://doi.org/10.1093/forestry/cpag041
Review